LRP 619/98 October 1998

Papers presented at the

20th Symposium on Fusion Technology

S O F T

September 7 - 11, 1998

Marseille, France

LIST OF CONTENTS

NEW DESIGN FOR THE ANODE POWER SUPPLY OF A GYROTRON

D.Fasel, S. Alberti, A. Favre, A. Perez, J. Acero*, D. Ganuza*, I. Garcia*, C. Lucia*

Centre de **R**echerches en **P**hysique des **P**lasmas, Association Euratom - Confédération Suisse
Ecole **P**olytechnique **F**édérale de **L**ausanne, PPB, CH - 1015 Lausanne, Switzerland

*JEMA S.A., E-20160 Lasarte-Oria, Spain

The introduction will remind the main supply structure installed in the CRPP, related to the ECRH (**E**lectron **C**yclotron **R**esonance **H**eating) project on the TCV (**T**okamak à **C**onfiguration **V**ariable) tokamak. Then this paper concentrates on the description of the power source designed to supply the anode of the triode type gyrotron. First the requirements asked for this power supply will be presented, taking into account the possible feeding structures in relation with the existing HV DC cathode power supply. The following section will focus on the selected design, describing in details the power structure based on MOSFET, referred to the cathode potential. Afterwards the control electronics is presented, including the feedback control implemented, the HV measurements, the internal reference generator and the interface to the TCV control. Finally, the last section will give information on the project status.

1. INTRODUCTION

For ECRH project on the TCV tokamak, it is planned to implement a system operating at both the 2nd harmonic (**3 MW @ 82.7 GHz**) and the 3rd harmonic (**1.5 MW @ 118 GHz**). At present the 2nd harmonic system has been completed. It is composed of **6** gyrotrons operating with a diode gun and delivering 500 kW each, for a pulse length of 2 sec. In this current year, the 3rd harmonic system will be installed. It is made up of **3** triode type gyrotrons, designed to deliver 500 kW each, for a pulse length of 210 sec, but used in CRPP according to the 2 sec pulse length of TCV. Details on the gyrotron itself are given in [1]. The general supply structure is presented in the figure 1.The double anode electron gun of these three gyrotrons allows the complete system to be fed by a common main power supply, while the generation of the RF power can be independently controlled through the anode voltage. Two power sources are available: either the 50 Hz network used mainly for the commissioning and conditioning of the gyrotrons, or the motor generator, which feeds TCV during the plasma shots. The DC HV (High Voltage) feeding the cathode of three gyrotrons is a solid state power supply based on IGBT, which has already been described in [2].

2. ANODE SUPPLY STRUCTURE

Few possibilities exist to energise the gyrotron's anode with the desired voltage. In the following paragraph the main requirements, imposed by the gyrotron's design, are described, as well as the two layouts proposed in the call for tender.

2.1 The main requirements

First of all, a list of the main electrical parameters defining the nominal working area of the gyrotron is drawn up:

→ The range of the differential anode-to-cathode voltage:

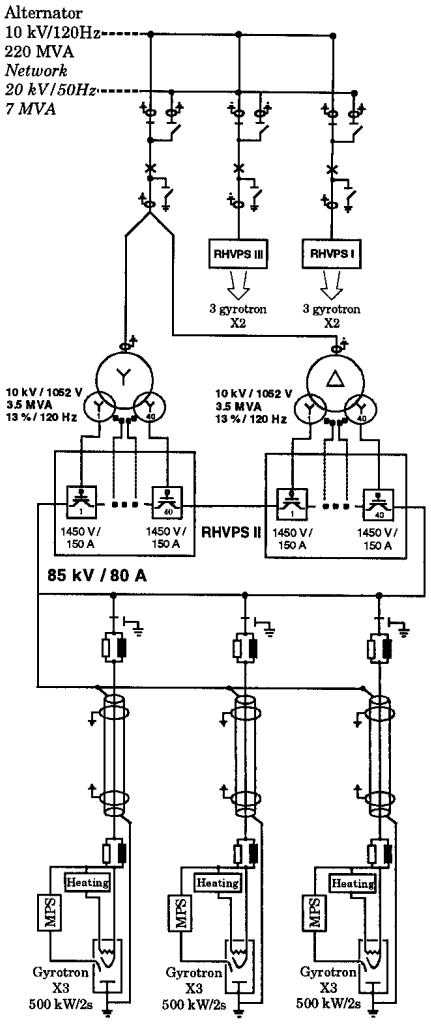

Figure 1: Part of the TCV power supply network

-5kV, ensuring the blocking state, to **30 kV**.

→ The anode current in static mode: **10 mA**. This value does not include the additional current to be drawn during transients, essentially due to the stray capacitance of the connection cables. The estimated value, in relation with a minimum transient time, is **250 mA**.

The output voltage of the power source must satisfy with the minimum transient time defined below:

→ From 0V to 30 kV, the minimum rise time of the output voltage, including the settling time, is **150 µsec**.

→ The higher frequency required for the output voltage modulation is 10 kHz, so the min rise time, considering a voltage range of 5kVpeak-to-peak, is **20 µsec**, including the settling time.

In case of severe faults in the gyrotron or in one of these auxiliaries, the following conditions must be fulfilled:

→ The max blocking time, defined as the duration for the output voltage to reach the blocking level starting from the nominal value, is **10 µsec**.

→ The energy dissipated in the gyrotron must be limited to **10 J**

2.1 The "derived" structure

One of the proposed layouts allows energising the gyrotron's anode from the cathode power source, as shown in the figure 2b. Actually, most of the modulators in use are based on this structure. Several possibilities exist to apply the desired voltage on the gyrotron's anode. The simplest is made of a resistive divider, which gives a constant ratio of the cathode voltage. This principle is only useful for the basic tests. In a more elaborated solution, active components, for example tubes, replace the passive ones (resistors). At the price of the complexity, the control of these active parts allows to apply on the anode a desired voltage, partly independent of the cathode voltage. A compromise consists in replacing only one of the resistor by an active component. So this solution is cheaper and easier to implement, but more restrictive considering the performances during transients.

This type of layout integrates a HV part, which is very simple and robust. But the auxiliaries required to operate the HV tubes (bias supplies, amplifying tubes, etc.), the losses and the associated cooling system, are heavy. Regular maintenance and adjustments are necessary. These arguments may influence the choice during the tender's evaluation, considering a tokamak experiment using several gyrotrons for heating purpose.

An other weakness of this structure is the existing time constant, due to the product of R_c with C_a & C_{ak} (stray capacitance represented in figure 2), which could be a limitation in front of the transient requirements.

2.2 The "stand alone" structure

The layout presented in the figure 2a shows a second possibility to feed the gyrotron's anode. The anode and cathode voltages are completely independent, except a galvanic link imposing that one polarity of this "stand alone" power supply is referred to the cathode potential.

In this configuration, a

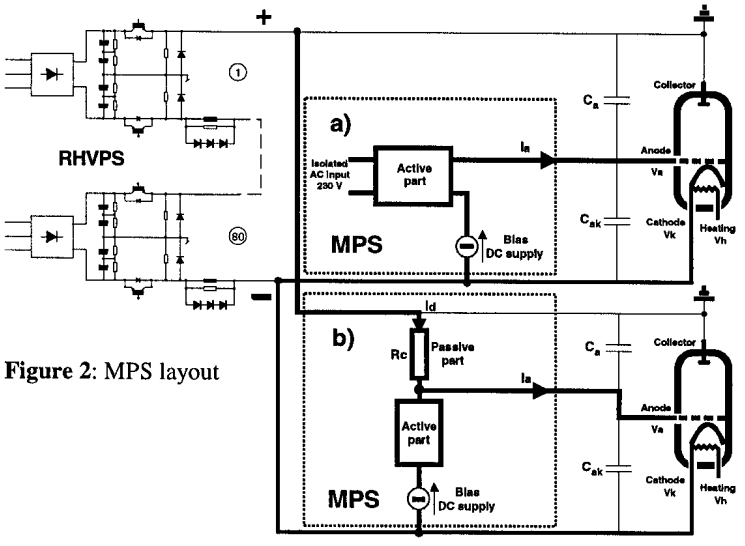

Figure 2: MPS layout

source is required, isolated at least at the cathode potential, in order to drawn the energy used by the HV assembly. As the cathode filament heating power supply requires also such a source, it can be used as the main source for the two assemblies.

This type of design is more adapted to semiconductors, for which the driving energy consumption is much lower than for tubes. Moreover, the progress made in the semiconductors technology leads to spare some place, which could be interesting in an HV environment.

Using this principle, the Vk and Vak voltages can be changed independently, without generating undesired transients on each other during the transitions. This argument is still more accurate if we consider that the cathode of three gyrotrons is fed by a common power source, as it is the case in CRPP.

3. THE MODULATOR POWER SUPPLY

In the MPS's (**M**odulator **P**ower **S**upply) call for tender, the suppliers were free to choose one of the layout proposed in the figure 2, as well as the power technology (tubes or semiconductors), so long as the technical requirements are fulfilled. Finally the offer from JEMA (Spain) was selected and the outline of the project is given underneath.

3.1 General description

The design, defined by JEMA's company, consists of two separated parts, which are presented, in the figure 3. The power part, surrounded with a dashed line on the drawing, is referred at the cathode potential and is formed of the HV parts, including its driving electronics and its auxiliaries. The control electronics referred at the ground potential.

The HV assembly is laid on isolators foreseen to sustain a DC voltage to ground of 150 kV. The mechanical structure is made of conductive material, reducing the influence of fast transients on the electronic. The overall is at the cathode potential and is placed as close as possible of the heating tower (see [2] for details), from where this potential is directly drawn. The isolated 230V AC supply used to supply the HV components as well as the necessary driving prints, is provided by the isolation transformer already existing in the heating assembly.

The control electronics is placed in a 19" rack, outside the HV zone. So the access to the reference, the measurements and the interlocks is possible according to the human safety rules, considering that the connections to the HV part are achieved by fibre optic links only.

3.2 MPS HV assembly

As shown in the figure 3, several stages are assembled in order to obtain the desired DC output voltage from the isolated AC 230V. Each of them are described in the following section:

The first stage (1) is intended to rectify the AC voltage and to filter the generated output voltage. The stored energy in the capacitor filter is also used to draw the current of the unavoidable stray capacitance during the output voltage transients. Furthermore, this unit ensures a power factor as near as possible of $\cos\varphi = 1$.

The following stage (2) is an H bridge converter, based on MOSFET semiconductors. From the DC voltage, a square AC voltage is generated at a constant frequency of 20 kHz. The block drawn on the diagram is effectively composed of two H bridges, working in parallel with a phase shift of 90°, in order to decrease the ripple after the rectifying diodes. The conduction duty cycle being constant, so only the ON/OFF commands are achieved in order to drive these units.

Afterwards, transformers (3) are used to raise the voltage up to the DC value required after the diodes rectifiers (4). Thus, a two polarities HV DC source is available, with a DC output voltage in the range –5kV to 30kV, referred at a common middle point.

The last stage (5) is formed by two groups of 60 MOSFET connected in series, used as regulated voltage sources. These additional semiconductor parts are imposed by the necessity to be bi-directional in current in order to generate and absorb the leakage current of the stray capacitance

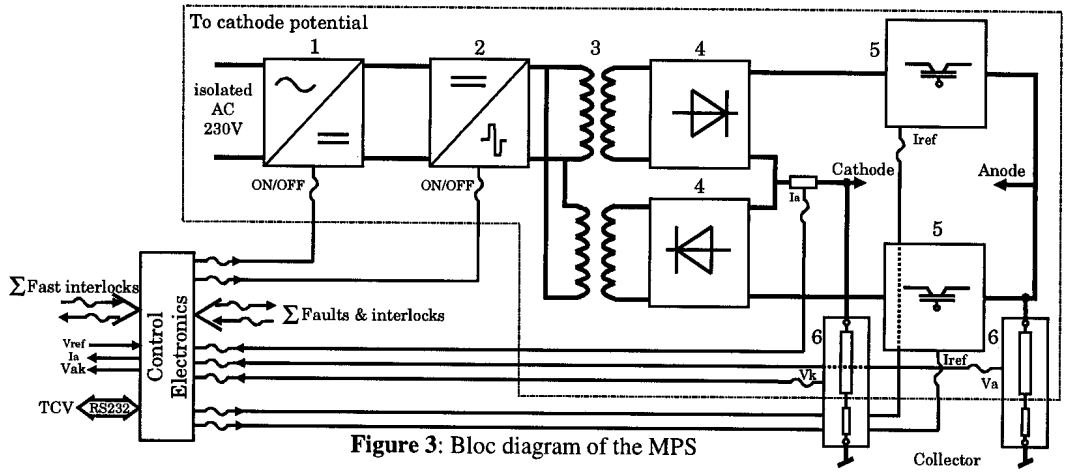

Figure 3: Bloc diagram of the MPS

during transients, such functionality being not realised with only the diode rectifiers. Each MOSFET is placed on a print implementing the local feedback loop and ensuring the equal sharing of the voltage on the semiconductors in series. Each print receives the current reference, used in the feedback loop, through an isolated cable inducing an image current in a secondary winding soldered on the print and isolated for the nominal anode's voltage. Such principle realises both the reference isolation and a synchronised reference distribution. A similar behaviour is used to supply each isolated print.

3.3 Control and measurement

Several tasks summarised hereafter are integrated in the electronics part:

→ The interface to the main control of TCV, through a RS-232 link and a bitbus connection, used to read the slow interlocks and to write the customer parameters, generating the internal voltage reference, like: the ramp-up time, the pulse length, the flat top value, the modulation's frequency etc.

→ The PID regulator on the Vak voltage, which output is converted through an A/D converter and transmitted to the HV assembly by an optical link, after a parallel to serial conversion. A clock signal is also transmitted to synchronise the emitter and the receiver.

→ The fast optical interface for I/O fault signals, which are used to block the HV in case of severe faults in the gyrotron or in the power supplies themselves.

The voltage measurements are realised with compensated resistor dividers (6). The Va and Vk voltages are measured separately and are combined through differential amplifiers in order to obtain the Vak voltage. The current measurement is supplied by a shunt, placed on the cathode polarity. The transmission of the measured values is achieved to the electronics with the same optical link as used for the MOSFET's reference.

4. STATUS OF THE PROJECT

Actually all the main parts forming the HV assembly have been tested and the mechanical structure is under construction. The MOSFET prints, dedicated to the output voltage regulation, have worked correctly on dummy load, in static conduction mode as well as in transients. These results are consistent with several case simulated under SPICE and EMTP. The further stage is to assemble the complete HV equipment and to test it with the control electronics.

REFERENCES

[1] M. Pain and al., Testing of the 118 GHz-quasi CW gyrotron for the Tore Supra and TCV tokamaks, this conference

[2] D. Fasel and al., Design and operation of..., SOFT 1996, vol.1, p.569-572

This project is partly supported by Swiss National Science Foundation

A NEW FLYWHEEL FOR THE TCV TURBO-GENERATOR

A. Perez, E. Baumont°, P. Bey°, R. Chavan, C. - W. Hustad** , D. Fasel, A. Favre, F. Picard°, J.-J. Simon*, H. Sprysl~

Centre de Recherches en Physique des Plasmas, Association Euratom - Confédération Suisse
Ecole Polytechnique Fédérale de Lausanne, CH - 1015 Lausanne

* DE LEME - EPFL, CH - 1015 Lausanne / ** DGM LTT - EPFL, CH - 1015 Lausanne
° TECHNICREA, F - 90000 Belfort / ~ ABB - KWHT, CH - 5400 Baden

The energy required for TCV tokamak pulses is provided by a turbo-generator. The planned increase in the plasma pulse length together with the installation of long pulse gyrotrons will lead to an increase of the energy demand. The extractable energy has been doubled by coupling a flywheel to the generator.

Introduction The early design of the TCV tokamak and its power supply system was based on a plasma pulse length of 1 s and provision of 20 MW was made for ECRH heating during 0.5 s [1], [2]. A turbo-generator was chosen to provide the required pulsed power and energy. At the beginning of the TCV operation, we noticed that the plasma pulse length could be increased to more than 2 s, with the available flux swing and without excessive coil heating. As a consequence, the ECRH system was designed with 2 s pulse length gyrotrons instead of the 0.5 s originally planned [3]. This upgrade did not result in additional electrical power demand but the extension of the plasma and the ECRH duration, lead to an energy consumption per discharge in excess of the 120 MJ available. The generator has thus been upgraded with a flywheel which allows for a total extractable energy of 240 MJ.

Generator description The generator (see Table 1 for main characteristics) was delivered by ABB in 1989. At that time, the generator design included the future possible addition of a flywheel. The rotor is provided with a coupling flange, the drive-end bearing is dimensioned to support one of the flywheel ends and the foundation is constructed such that a flywheel could be installed. The generator drive system provides a maximum of 1.8 MW. Accounting for generator losses of 1196 kW at 3600 rpm, acceleration between pulses is possible in a time of 2 min. using the remaining 600 kW.

Table 1: Generator main characteristics

Machine type	turbo, air cooled, 4 poles
Nominal voltage / current / power	10 kV / 12. 5 kA / 220 MVA, 3.5 sec every 300 sec.
Short-circuit power at 2900 rpm	1500 MVA
Speed / frequency range for the pulse	3600 - 2900 rpm / 120 - 96 Hz
Stored / extractable energy	341 MJ at 3600 rpm / 120 MJ, 3600 - 2900 rpm
Stator / rotor weights	100 tons / 36 tons

Flywheel description The flywheel call for tender was issued in June 1996 and an order was placed to Technicréa, Belfort - France, in December 1996. One of the main technical challenges was to maintain the flywheel losses below 200 kW in order to limit the increase in operational cost, and to retain sufficient acceleration power for a full energy pulse every 10 min. The solution proposed by Technicréa exploited the capability of the generator bearing to support one of the flywheel ends, thus saving the losses of a fourth bearing. The generator rotor and the flywheel are then supported on three bearings only (see Figure 1). The flywheel (see Table 2 for technical specification) runs under partial vacuum in order to minimise ventilation losses.

Table 2: Flywheel main design characteristics

Overall length, drum length, diameter	2680 mm / 1600 mm / 1400 mm
Stored / extractable energy	340 MJ at 3600 rpm / 120 MJ, 3600 - 2900 rpm
Flywheel / housing weights	20 tons / 2.5 tons
Nominal vacuum	200 mbars
Ventilation losses / bearing losses	25 kW / 40 kW

Flywheel rotor The flywheel is machined in a single forged piece of high quality alloy steel (26NiCrMoV145), with Re 0.2% higher than 750 N/mm2. An axial bore has been made to allow for verification of the steel characteristics in the flywheel centre. Technicréa has performed extensive calculations of the complete shaft line with its three bearings in order to identify the bending eigenmodes and to check that none of them is situated within the range of pulse speed. Bearings vibrations and loads have been calculated for different imbalances located at the generator rotor and / or the flywheel. Finite elements calculations have been used to analyse the stresses due to centrifugal forces and temperature gradients in the flywheel. The maximum stresses obtained have been checked to comply with low cycle fatigue criteria for the required 150'000 pulses and 20'000 starts. All the stresses are well below the material capability, with the exception of the stress appearing at the bottom of the central bore. Technicréa has analysed this zone from the point of view of Fracture Mechanics, concluding that in the case of fatigue crack initiation, the crack dimensions would remain well below critical levels.
Using the method of Boundary Elements to compute stresses, ABB has also made similar calculations. Their finding largely confirm the results of Technicréa with the exception of somewhat higher constraints, mainly at the central bore.

Torsion A rigid coupling is required to allow for the flywheel to be supported by the generator bearing. A torque up to 350 kNm is transmitted by friction between coupling flanges. Considering the shear limit of the coupling bolts, a torque of 3500 kNm, which is also the shaft limit, could be exceptionally transmitted. Torsional resonances are also found for the shaft line. Calculations situate the first mode at 24 Hz with all others being located at frequencies > 137 Hz. In the case of oscillation at the fundamental frequency, the main torsional stress will be located in the shaft. The torsional behaviour of the system has been analysed by Technicréa and ABB for tokamak discharges and generator short-circuits. The torque resulting from typical tokamak pulses is calculated to remain below 350 kNm. A short-circuit at nominal voltage, would result in an electrical torque as high as 8000 kNm. This could only happen, however, within the pulse speed range where the frequency of the pulsating torque is much higher than the fundamental mode, resulting in a shaft torque of 1500 kNm. The torsion becomes dangerous if the applied pulsating torque is at the fundamental frequency. This could only occur in two ways; in case of a generator short-circuit at 720 rpm, or if, during the pulse, some of the TCV coil currents begin oscillating at 24 Hz. During start-up or braking sequences, the generator voltage is much lower than nominal and corresponds to 620 V at 720 rpm. This would result in a pulsating torque of 500 kNm

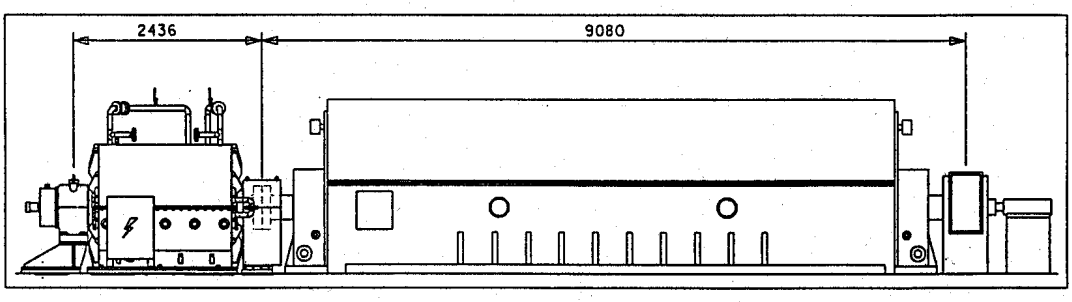

Figure 1: Generator and flywheel layout

in case of short-circuit. This case has been qualified as very improbable but most dangerous and has been studied by Technicréa. The pulsating torque being synchronised with the torsional resonance and the mechanical damping being very low, the shaft torque would be incremented by 500 kNm for each half period, thus reaching 3500 kNm after 140 msec. The Electromechanics & Electric Machines Laboratory (LEME) at the EPFL has performed a precise calculation of the electrical short-circuit torque. Using the SIMSEN software developed at the LEME, the maximum electrical torque is predicted to reach 450 kNm and to decrease with a time constant of 120 msec. Technicréa, who considers a similar damping of the electrical torque, find that the resulting torque in the shaft saturates at 3200 kNm after 600 msec. Even if the security margin is rather small, we conclude that the system is intrinsically safe for this case. A TCV pulse with coil currents at 24 Hz is also improbable but there is no intrinsic limit to the torque which could be reached.

Casing The casing consists of a sandwich structure fabricated in stainless steel through which the cooling water flows. It is designed and tested to withstand internal vacuum together with a water pressure of 8 bars. The gap between flywheel and casing is of 50 mm.

Losses In order to limit the ventilation losses to 25 kW, Technicréa proposed that the flywheel run in a closed casing (without external air flux) under a partial vacuum of 200 mbars. Various simulations and analytical calculations have been performed to estimate the losses under vacuum, to choose the gap between casing and flywheel and to verify the thermal behaviour of the system. Both ABB and the EPFL Lab. of Applied Thermodynamics and Turbomachinery (DGM-LTT) performed similar calculations. All findings were consistent regarding the losses. From the thermal point of view, however, important differences were identified. Table 3 lists the main results obtained. An accidental loss of the vacuum when running at nominal speed has also been analysed. If this occurs, Technicréa concluded that the air temperature in the gap would rise up to 240 deg C, which can be withstand by the chosen vacuum pump. Simulations have been performed to compute the temperatures and thermal stresses in case of shutdown with loss of vacuum and cooling water circulation. Fortunately, since the generator losses are much higher than those of the flywheel, only 10 % of the total stored energy is dissipated by air friction within the flywheel casing. The calculated temperature rise and gradients are well below the acceptable limits.

Protection To monitor the torsional stresses, the shaft is equipped with a strain gauge in order to continuously measure the torque and to allow for machine shutdown in the case of threshold overshoot. The sensitivity of the generator over-current protection during start-up and brake sequences has also been improved. In view of the general lack of experience of similar systems running under vacuum, the flywheel casing is fitted with 11 ports giving access to the internal gap and allowing, if required, for the installation of pressure, temperature and air velocity sensors. Two infrared temperature sensors, an air temperature sensor and two vacuum sensors monitor continuously the flywheel surface temperature, the air temperature and the vacuum in the gap. A vibration sensor is also fixed to the flywheel bearing. The machine will be shutdown if one of these measurements exceeds its threshold limit.

Factory test The flywheel was balanced and an overspeed test at 4300 rpm successfully passed at the GEC - ALSTHOM factory in Belfort. Together with its bearing and a provisional one,

Table 3: Ventilation losses calculated

	TECHNICRÉA	ABB	DGM-LTT
1000 mbars / 150 mm gap	-------	75 kW	110 kW
1000 mbars / 50 mm gap	90 kW	-------	121 kW
200 mbars / 50 mm gap	21 kW	-------	32 kW
Steady state temp. difference flywheel surface / casing	96 °C at 200 mbars and 50 mm gap	80 °C at 1000 mbars and 150 mm gap	30 °C at 1000 mbar and 50 mm gap

casing and vacuum pump, the flywheel was mounted on a test platform in order to verify the predicted losses and thermal behaviour of the system. The flywheel bearing losses were confirmed to be 39 kW for 3800 rpm and the ventilation losses investigated at various vacuum levels and speeds. Figure 2 shows the ventilation losses alone at 3800 rpm as a function of the vacuum pressure. Extrapolating to 0 mbar yields a loss of around 30 kW which is expected to be generated by the ventilation effect of the coupling flange and the bolts and the different shafts placed between the DC drive motor, the gear and the flywheel.

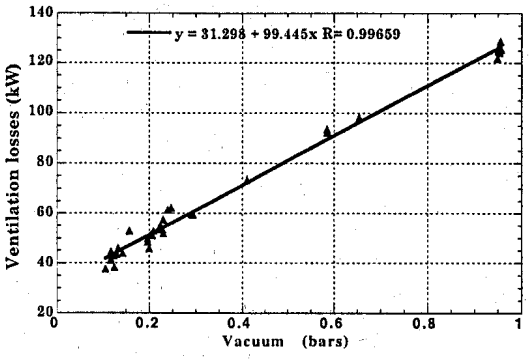

Figure 2 Flywheel losses at 3800 rpm

Operation after installation The generator together with the flywheel have been commissioned in June 98. As a result of small misalignment, the flywheel has been re balanced on site. The vibrational behaviour of the system is not always reproducible making improvement difficult. It appears that the relative temperatures of different parts of the machine have an impact on the vibrations and result in displacement amplitudes which depend not only on the speed but also on the running period and the duration of the standstill period. Whilst the vibration amplitudes are not yet below the 6 μm peak-to-peak specified for the pulse speed range, they remain below 20 μm pp considered, according to standard rules for industrial machinery, as good. Efforts are still underway in order to improve the vibration level. The torque monitoring system has shown the existence of 50 to 100 kNm peaks when crossing the speed levels of 60 and 120 rpm. These are due to resonance with the 12th and 6th harmonics of the drive invertor. A further peak (lower than 50 kNm) which appears when crossing 2880 rpm, has not yet been explained. In order to test the torque measurement, some pulses have been triggered with a 24 Hz current on a TCV coil. The measured torque amplitude and the reaction time of the protection logic have been checked.
Just after installation, the drive converter needed, to maintain the machine at 3600 rpm with 240 mbar of vacuum, 103 kW more than before installation of the flywheel. Later on, a cover has been placed on the coupling bolts, resulting in a reduction of the drive power supplement to 84 kW. This value includes the additional losses of the generator drive end bearing due to the 10 tons of additional load, the flywheel bearing losses, found during the factory tests to be 39 kW, and the flywheel ventilation losses. Figure 2 shows that with a vacuum of 200 mbars, there will be a reduction of 4 kW in the ventilation losses, resulting in a total of 80 kW due to the flywheel installation alone. The flywheel surface temperature which has been measured during factory and site tests has kept below 50 °C, thus confirming the DGM-LTT calculations.

Conclusion It has been possible to double the extractable energy of the TCV generator by adding a flywheel. The losses have been increased by only 7 %. The factory tests as well as the site tests have demonstrated that the chosen design will keep its promises.

Acknowledgements The authors wish to thank many contributors from the CRPP, from the EPFL, from Technicréa, from ABB and from many other companies in France and in Switzerland who have helped this challenging project to reach a successful conclusion.
This work is partially supported by the Swiss National Science Foundation.

References

[1] Perez A., A 220 MVA turbo generator for the TCV tokamak, SOFT 1988, vol. 2, p. 1449-1453
[2] Fasel D., 19 rectifiers to supply the coils of the TCV tokamak, SOFT 1990, vol. 2, p.1492-1496
[3] Fasel D., Design of the power installation for the TCV ECRH, SOFT 1996, vol. 1, p. 569-572

Plasma Modelling for Position and Shape Control in TCV

P.Vyas[1], R.Albanese[2], G.Ambrosino[2], M.Ariola[2], I.Bandyopadhyay[3], A.Coutlis[4], D.J.N.Limebeer[4], J.B.Lister[1], F.Villone[2], J.P.Wainwright[4]

[1] Centre de Recherches en Physique des Plasmas, Association Euratom-Confédération Suisse, Ecole Polytechnique Fédérale de Lausanne, Lausanne, Switzerland
[2] Associazione Euratom-ENEA-CREATE, Dipartimento di Ingegneria, Università di Napoli, Naples, Italy
[3] Institute for Plasma Research, Bhat, Gandhinagar, India
[4] Centre for Process Systems Engineering, Imperial College, London, United Kingdom

ABSTRACT Results are presented from the system identification of the open loop response of the plasma shape and position on TCV. Comparisons with white box, black box and grey box models have been made.

1 INTRODUCTION

Many tokamak plasma position and shape control systems have been based on simple models of the plasma and relatively basic PID controllers. In most cases the system performance is adequate but could be further improved by the use of modern control strategies. However this benefit comes only when a suitable model of the system is available. The model should typically be linear or linearized about an operating point. An advanced control strategy of this type has been proposed for use on ITER. The aim of this paper is to examine various options for plasma response modelling. The TCV tokamak is ideal for this type of study since it has 18 independently powered poloidal field coils and operates with a wide variety of plasma shapes.

Three different approaches to modelling the plasma response to control coil stimulation have been studied on TCV. One approach is to develop *a priori* models derived from physical laws and this is known as 'white box' modelling. One example is the CREATE-L model [1] which has been shown to be in close agreement with closed loop validation experiments on TCV [2,3]. A second 'black box' approach is to excite the plasma response with externally generated stimulation signals. A model is then obtained from a mathematical fit to the data. A third method ('grey box') is to develop a physical model in which many of the parameters are known, and to use the experimental data to fit any unknown or uncertain parameters. This article describes the method and results for system identification of the plasma shape and position response, and the development of a simple grey box model.

2 SYSTEM IDENTIFICATION

The aim of the identification procedure is to model the dynamics between the input demand voltage at the PF power supplies and the plasma electromagnetic control parameters. We consider the power supply to be part of the open loop TCV system and thus seek to identify a model for $G(s)$ in Fig. 1. Measurements of the voltage commands to the power supplies ($\boldsymbol{u}$) and of the control parameters ($\boldsymbol{cp}$) are available. There are five electromagnetic control parameters used in these discharges: P_VERT (the radial flux imbalance) which is a measure of radial position, TRI_OUT (the outboard field curvature) and TRI_IN (the inboard field curvature) which together define elongation and triangularity, I_p (the plasma current) and zI_p (the product of the plasma current and the vertical plasma position). Another parameter not under feedback control but considered here is Ψ_R, the difference between the R^2I_p and $R_0^2I_p$ current moments, where R_0 is the unperturbed major radius. All these parameters are estimated using linear combinations of fluxes,

poloidal fields, and poloidal field coil currents (I_{pol}). In almost all cases they are a more sensitive test of the plasma dynamics than the raw magnetic fields and fluxes, since they are generally differences between terms dominated by the plasma-less response rather than the plasma response. A multi-input multi-output, proportional integral derivative controller (PID), acts through all coils, stabilizes the plasma position and regulates the control parameters using thyristor power supplies (PS). The K1 and K2 blocks represent feedback matrices. Further details are reported in [4].

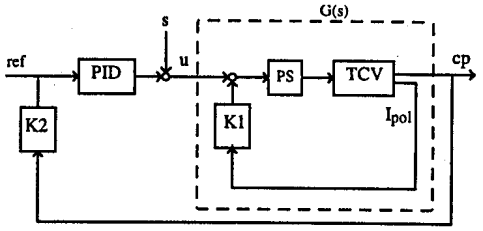

Fig. 1 TCV control loop.

2.1 Experimental procedure

A weakly shaped plasma with a low vertical instability growth rate (~200 s^{-1}), implying a low open loop bandwidth, was considered to be more suitable for this first experiment. The main parameters were R=0.87 m, a=0.22 m, B_ϕ=1.4 T, I_p=200 kA, κ_{95}=1.4, δ_{95}=0.23, q_a=4.6, n_e=2.2×10^{19} m^{-3}. The plasma was up-down symmetric, limited and centred at the midplane. The PF coils were driven in up-down symmetric pairs, exploiting the symmetry of the equilibrium to improve the signal to noise ratio of the responses. This led naturally to a decoupling of the plasma responses because anti-symmetric stimulation produces a purely radial field on axis, driving only zI_p.

During each identification experiment, measurements of the input and the output of the plant system were taken at 5 kHz over a time interval of 0.5 s. An initial period of 50 ms was discarded to remove the effect of the initial transient response. The excitation signal was composed of 29 sine waves spanning the angular frequency range 20 rad/s to 3000 rad/s. The slowest sine wave is resolvable given the pulse length, and the highest excitation frequency was designed to be below half the sampling frequency and also above the assumed TCV bandwidth. The sine wave phases were chosen to minimise the maximum amplitude of the total signal. The frequencies are close enough so that resonant peaks or notches were not expected to be missed and the open loop bandwidth of the system was spanned. The amplitudes of the higher frequency sine waves were increased to compensate for the lower gain of TCV at these frequencies. The test signal was scaled to ensure that power supply constraints were avoided. The same excitation signal was applied to all the symmetric and anti-symmetric coil pair combinations, producing a total of 18 experiments.

2.2 Frequency response estimation

The 29 sine wave components are measured in the input (u) and output (cp) data using a generalized DFT. To identify a 1-output, q-input system we need to have performed q experiments. For the j^{th} experiment we define the input frequency spectrum as $U_l^j(\omega_i)$ and the output frequency spectrum as $Y^j(\omega_i)$, where l indexes the inputs. An estimate of the system frequency response at each measurement frequency is given by,

$$\hat{G}(\omega_i) = \begin{bmatrix} Y^1(\omega_i) \\ \vdots \\ Y^q(\omega_i) \end{bmatrix}^T \begin{bmatrix} U_1^1(\omega_i) & \cdots & U_q^1(\omega_i) \\ \vdots & \ddots & \vdots \\ U_q^1(\omega_i) & \cdots & U_q^q(\omega_i) \end{bmatrix}^{-1}.$$

The invertibility of the input matrix at each frequency is a mild assumption that is satisfied if the corresponding matrix for the designed test-signal is invertible. If that is the case, then the experiments performed are said to be independent. This invertibility is satisfied with our coil-pair stimulation experiments since the condition numbers of this matrix lies in the range 3 to 30.

3 WHITE BOX MODEL

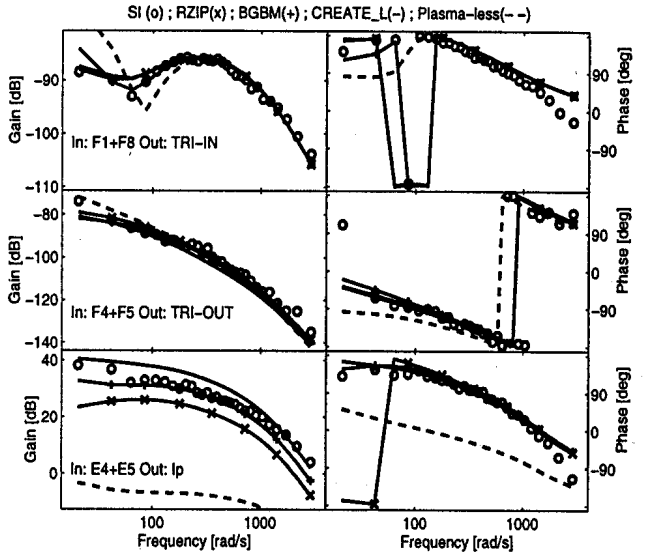

Fig. 2 System identified frequency responses (circles), CREATE-L (line), plasmaless model (dashed), BGBM ('+') and RZIP model with nominal parameters ('×')

The frequency point estimates of the open loop transfer function can be compared directly with the CREATE-L model. In general the CREATE-L model agrees with the experimental estimates to within the variance of the estimates (41 cases out of 50). A typical case, Fig. 2, has frequency estimates with a variance of approximately 1 to 2 dB in the amplitude response and less than 5° in the phase response. Typically the model-experiment difference is of the same order as the variance of the experiment estimates. Even though the responses can span a very large dynamic range, over 50 dB, the agreement is still good. This is especially remarkable at high frequencies with very low gains. The variance of the experimental frequency response estimates varies according to the choice of input-output pair. However for each pair it remains roughly constant in dB units across the range of frequencies. When the variance is low, the agreement between the models and the data is generally good and there is normally no variation between the models. The phases rotate smoothly as the frequency increases. At the highest frequencies, the response gain is usually small and the amplitude and phase become more uncertain. There are too few cycles of the lowest frequency stimulation to obtain an accurate measurement and these data show a regularly large departure from a smooth frequency dependence. Thus the lowest frequency data have been disregarded.

In some rare cases clear differences between the CREATE-L model and the data can be observed (Fig. 2). These discrepancies only occur for some of the I_p and Ψ_R responses. This was not previously seen in closed loop responses [2,3] and highlights the role of the feedback system in reducing the sensitivity of the performance of the closed loop system to changes in the response of the open loop system.

4 BLACK BOX MODEL

The raw frequency response data can be used to fit the parameters of a mathematical model [5]. This was useful for the case of the anti-symmetric stimulation, for which a single low order multi-input single-output model can describe the response of zI_p. The model reduction procedure forces all anti-symmetric responses to have the same unstable pole, namely the vertical instability growth rate. However the symmetric response of the plasma is more complex, with different modes affecting different coils. As a result, low-order multi-input single-output models relating one control parameter to all PF coils could not be obtained. Models were constructed for individual input-output responses and then combined.

5 GREY BOX MODEL

A grey box model was developed for TCV to take advantage of both the experimental data and also well defined knowledge of the tokamak electromagnetic properties in the absence of plasma. The RZIP (R, z, I_p) model [6] has been developed from a set of circuit equations based on the supposition that the plasma current distribution remains constant during any control action, but that its centroid can move vertically and radially and its integral, the total plasma current, can change. This describes the dominant terms in the plasma response but neglects high orders effects for example on elongation and triangularity.

A very large number of coefficients, such as mutual inductances between active and passive coils, are not related to the plasma, and in principle can be accurately determined given the required effort. These values have been validated on TCV with vacuum PF coil tests. There are 4 other coefficients which are related to the plasma but which are largely insensitive to the current distribution. Their values can be calculated with some confidence. This leaves 6 remaining parameters which can be found using an optimization procedure to minimize the difference between the experimental response and the model. We chose a relatively simple measure of the error, summing the absolute value of the model difference over the frequencies, inputs, and control parameters *cp*. There is a weighting on each *cp* because they have different dimensions. The frequencies are weighted uniformly. The minimum of the cost function is found by a standard simplex minimisation procedure. The inital parameter values were set to zero. The model obtained using this approach is termed the BGBM (Best Grey Box Model).

Figure 3 shows the sensitivity of the cost function to changes in the parameters from their BGBM values. The plasma self-inductance (L_p) is the most sensitive parameter followed by M_{33} which defines the Shafranov equilibrium constraint. The vertical lines show values estimated from a reconstructed equilibrium. For the sensitive parameters these values lie close to the BGBM values. The BGBM-experiment difference is as good as the CREATE-L model. A visible improvement occurs in only 5 out of the 50 input-output relationships (Fig. 2).

6 CONCLUSIONS

System identification experiments have been performed on TCV and have successfully measured the open loop frequency response of the plasma position and shape to coil voltage stimulation. A grey box model has been developed which makes use of *a priori* knowledge of the vacuum response along with the experimental data.

ACKNOWLEDGEMENTS

This work was partly supported by Euratom mobility contracts (FV [ENEA] and AC [UKAEA]) and partly by the Fonds national suisse de la recherche scientifique.

REFERENCES

[1] Albanese, R. et al, Proc 19th SOFT, Lisbon, September 1996, vol. 1, p. 735
[2] Villone, F., et al, Nuclear Fusion, **37**, 1395-1410 (1997)
[3] Vyas, P., et al, Nuclear Fusion, in press (1998)
[4] Lister, J.B., et al, Fusion Technol., **32**, 321-373 (1997)
[5] Coutlis, A., et al., submitted to IEEE Trans. Applications Control Systems (1998)
[6] Coutlis, A., et al., CRPP Report LRP 606/98 (1998)

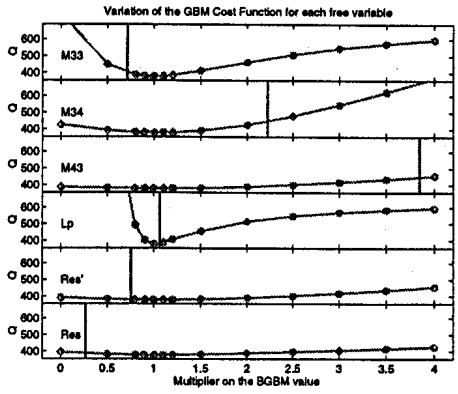

Fig. 3 Cost function variation with model parameters